www.sciencemag.org/content/343/6177/1363/suppl/DC1

Supplementary Materials for

Structure of the Mitochondrial Translocator Protein in Complex with a Diagnostic Ligand

Łukasz Jaremko, Mariusz Jaremko, Karin Giller, Stefan Becker,* Markus Zweckstetter*

*Corresponding author. E-mail: markus.zweckstetter@dzne.de (M.Z.); sabe@nmr.mpibpc.mpg.de (S.B.)

Published 21 March 2014, *Science* **343**, 1363 (2014)
DOI: 10.1126/science.1248725

This PDF file includes:

Materials and Methods

Figs. S1 to S9

Table S1

References

Materials and Methods

NMR spectroscopy

mTSPO was expressed in *E. coli* in M9 minimal medium and reconstituted into 2 % (m/v) DPC micelles according to published protocols (*11, 17, 27*). NMR measurements were carried out on 900 and 800 MHz NMR spectrometers at 42 ^{o}C for 0.5-0.9 mM protein solution in 10 mM sodium phosphate buffer, pH 6.0, in the presence of approximately 2% (m/v) DPC and 2.9 mM *(R)*-PK11195. Spectra were processed with the software TopSpin (Bruker) and analyzed using CARA (*29*). A total of 98% of all backbone resonances were assigned with the help of TROSY-based 3D HNCO, HNCA, HN(CO)CA, HNCACB, and HN(CA)CB experiments (*30-33*), which were recorded on ^{2}H,^{13}C,^{15}N-labeled mTSPO-(*R*)-PK11195. Backbone resonance assignments were further supported by NH-NH i ± 1, 2, 3 connectivities observed in a 3D ^{15}N-edited NOESY-HSQC spectrum (NOE mixing time of 200 ms) (*34, 35*). To resolve any remaining assignment ambiguities, complex samples with selected ^{13}C,^{15}N-labeled amino acids were prepared: ^{1}H,^{15}N,^{13}C-labeled for Ile, Lys, Gly, Pro ([U-^{2}H; U-^{1}H, ^{15}N,^{13}C-IKPG]-mTSPO) as well as Trp, Arg ([U-^{2}H; U-^{1}H, ^{15}N,^{13}C-WR]-mTSPO) with all other residues perdeuterated and natural abundance of carbon and nitrogen isotopes. For the selectively labeled samples, 2D ^{1}H-^{13}C HSQC, 2D ^{1}H-^{15}N HSQC, 2D TROSY-based HNCA and HNCO (^{1}H-^{15}N planes) spectra, as well as 3D ^{13}C-edited NOESY-HSQC (mixing time of 200 ms) and ^{15}N-edited NOESY-HSQC (mixing time of 200 ms) spectra were recorded. All fourteen Pro residues were in *trans* conformation on the basis of experimental C_{β} and C_{γ} chemical shifts according to PROMEGA (*36*).

Stereo-specific assignment of δ_1/δ_2 and γ_1/γ_2 methyl groups of valines and leucines, as well as distinction of δ_1/γ_2 methyls in isoleucines was achieved by analysis of 2D ^{1}H-^{13}C HSQC, 3D ^{15}N-resolved NOESY and 3D ^{13}C-resolved NOESY spectra recorded on a sample of [U-^{2}H,^{15}N; I$^{\delta1}$/LV^{proS}-^{13}CH$_3$]-mTSPO in complex with PK11195. NOE cross peaks between ^{13}CH$_3$ methyl groups and NH amides of the same spin system, which were observed in a 3D ^{13}C-edited NOESY-HSQC spectrum (200 ms mixing time) in H_2O, enabled the connection of the HN backbone resonances with their side chain methyl protons in all valine, isoleucine, and leucine residues.

The assignment of aliphatic side chain resonances was obtained using 3D (H)CCH-TOCSY, 3D H(C)CH-TOCSY (mixing times of 10 and 16 ms, respectively) (*37*) and 3D ^{13}C-edited NOESY-HSQC (200 ms mixing time) spectra recorded on ^{13}C,^{15}N-labeled mTSPO-(*R*)-PK11195 complex in D_2O, as well as a 3D ^{15}N-edited NOESY-HSQC spectrum (170 ms mixing time) measured in H_2O. Completion of the assignment of the side chain resonances of leucines and phenylalanines was possible using [U-^{2}H; U-^{1}H,^{15}N-LF]-mTSPO-PK11195 with selectively labeled leucines and phenylalanines, while [U-^{2}H; U-^{1}H,^{15}N,^{13}C-WR]-mTSPO-PK11195 was used for the side chain resonance assignment of tryptophan and arginine residues. For both samples, 2D ^{1}H-^{13}C HSQC and aromatic as well as aliphatic 3D ^{13}C-resolved NOESY spectra (200 ms NOE mixing time) were recorded. To further reduce signal overlap in 2D ^{1}H-^{13}C HSQC and 3D ^{13}C-edited NOESY-HSQC spectra and validate the aliphatic and aromatic side chain resonance assignments, a sample was prepared for which [2-^{13}C]-glucose containing medium was used as carbon source (*38*). All experiments together allowed assignment of more than 95% of ^{1}H, ^{13}C, and ^{15}N backbone and side chain resonances.

The ^{1}H resonances of the E- and Z-amide rotamer of (*R*)-PK11195 were assigned for the free ligand in 60 mM DPC-d_{38} using 2D ^{1}H-^{1}H NOESY spectra (NOE mixing times of 100 and 300 ms) recorded at 42 ^{o}C. The chemical shifts of the protein-bound ligand together with 61 protein-ligand NOE contacts were then assigned by comparison to the chemical shifts of free (*R*)-PK11195 in DPC and analysis of NOE strips in 3D ^{13}C- and ^{15}N-edited NOESY, 3D F1-^{13}C,^{15}N-filtered/edited-NOESY-^{1}H-^{13}C-HSQC, and 3D F1-^{13}C,^{15}N-filtered/edited-NOESY-^{1}H-^{15}N-HSQC spectra recorded on the TSPO-PK11195 complex (*39*). In the complex, PK11195 adopts the E-rotamer. Fixing the PK11195 amide to the Z-rotamer (φ_1 = 180.0 ± 10.0^{o}) resulted in violation of inter proton distances.

Structure determination

The overall topology of TSPO was determined on the basis of 305 manually assigned medium-range NH-NH contacts in the five transmembrane helices, 185 intramolecular long-range NOE contacts, which were observed between well-separated side chain methyl proton resonances and the tryptophane imidazole groups in 3D ^{13}C- and ^{15}N-edited NOESY-HSQC spectra (mixing times of 100 ms), as well as 61 ligand-to-protein contacts detected in 3D F1-^{13}C,^{15}N-filtered/edited-NOESY-^{1}H-^{13}C-HSQC and 3D F1-^{13}C,^{15}N-filtered/edited-NOESY-^{1}H-^{15}N-HSQC experiments (both 100 ms NOE mixing time). NOE cross peak intensities were calibrated and divided into four distance classes, as very weak 1.8-6.0 Å, weak 1.8-5.5 Å, medium 1.8-4.5 Å and strong 1.8-3.5 Å. The manually assigned medium- and long-range distance restraints were subsequently used together with a full set of cross-peaks from 3D ^{15}N- and ^{13}C-edited NOESY spectra (mixing times of 100 ms) for automatic NOE assignment and structure calculation in CYANA 3.0 (*40*). The structure calculation was supplemented by dihedral angle restraints predicted from experimental chemical shifts using TALOS+ (*41*), as well as 170 hydrogen bond restraints for 85 NH⋯O=C hydrogen bonds in the transmembrane helices based on experimental hydrogen/deuterium exchange profiles and supported by characteristic NOE contacts. Structure refinement was carried using a simulated annealing protocol implemented in XPLOR-NIH 2.33 (*42*).

Backbone dynamics

Picosecond-to-nanosecond motions of the TSPO backbone in complex with PK11195 were analyzed on the basis of ^{1}H-^{15}N steady-state NOEs (*43*) observed at 42 ^{o}C in U-[^{15}N,^{13}C]-mTSPO-PK11195 in 2% DPC-d_{38}, 10 mM sodium phosphate buffer, 90/10% H_2O/D_2O. In addition, RCI-S^2 order parameters were predicted from backbone chemical shifts observed at 42 ^{o}C (*44*).

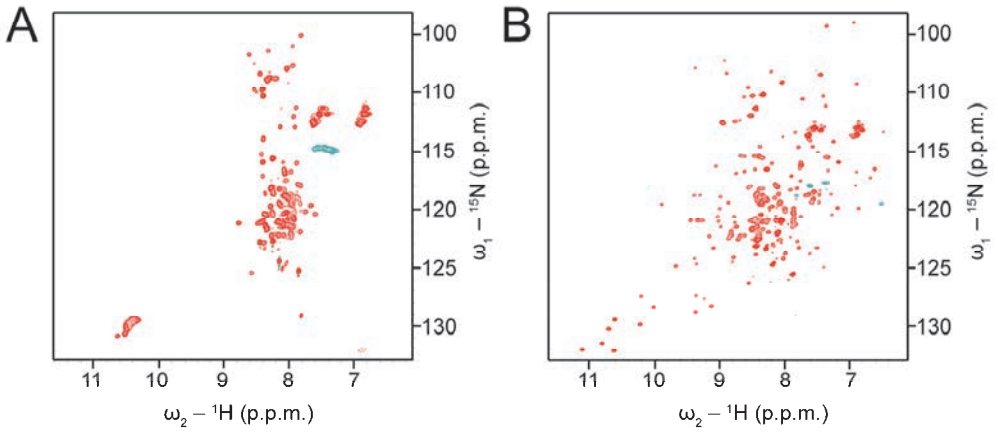

Fig. S1.

Ligand-induced stabilization of the mTSPO structure. Comparison of 2D ^{1}H-^{15}N HSQC spectra of mTSPO reconstituted into DPC micelles in the absence **(A)** and presence **(B)** of *(R)*-PK11195. Spectra were recorded on a 900 MHz NMR spectrometer at 42 °C using 0.8 mM U-[^{2}H,^{13}C,^{15}N]-mTSPO in 2% DPC-d_{38}, 10 mM sodium phosphate buffer. The concentration of *(R)*-PK11195 in (B) was 2.9 mM.

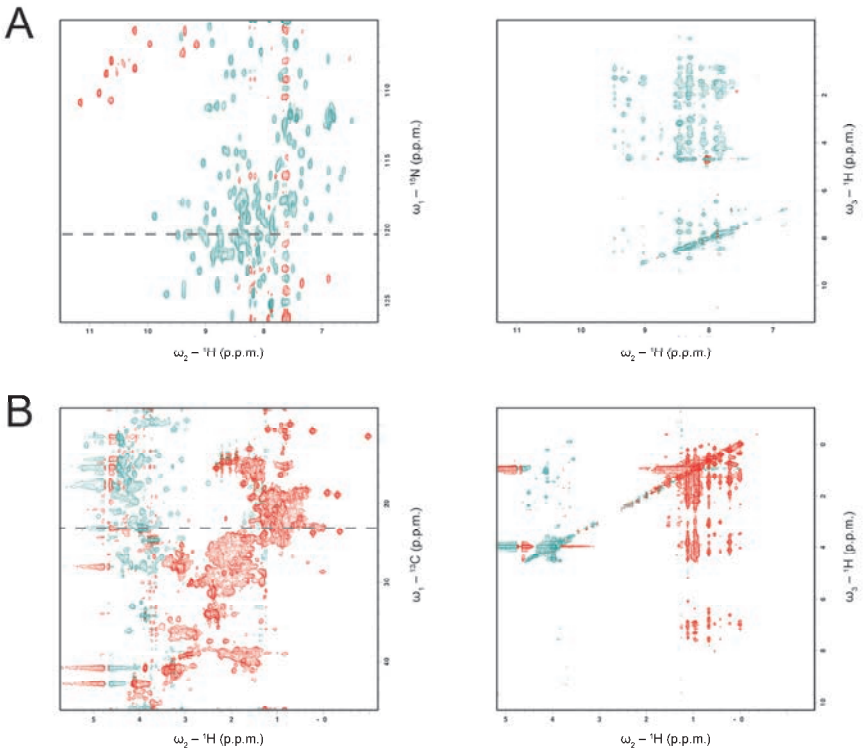

Fig. S2

2D planes and representative slices of 3D ^{13}C- and ^{15}N-edited NOESY-HSQC spectra recorded on the mTSPO-PK11195 complex. The 2D ^{1}H-X HSQC (X = ^{13}C or ^{15}N) planes and the corresponding 2D ^{1}H-^{1}H NOESY slices (taken at the position indicated by the gray dotted line on the plane) from **(A)** the 3D ^{15}N-edited NOESY-HSQC (NOE mixing time of 100 ms) and **(B)** the 3D ^{13}C-edited NOESY-HSQC of the aliphatic region (NOE mixing time of 100 ms) are shown.

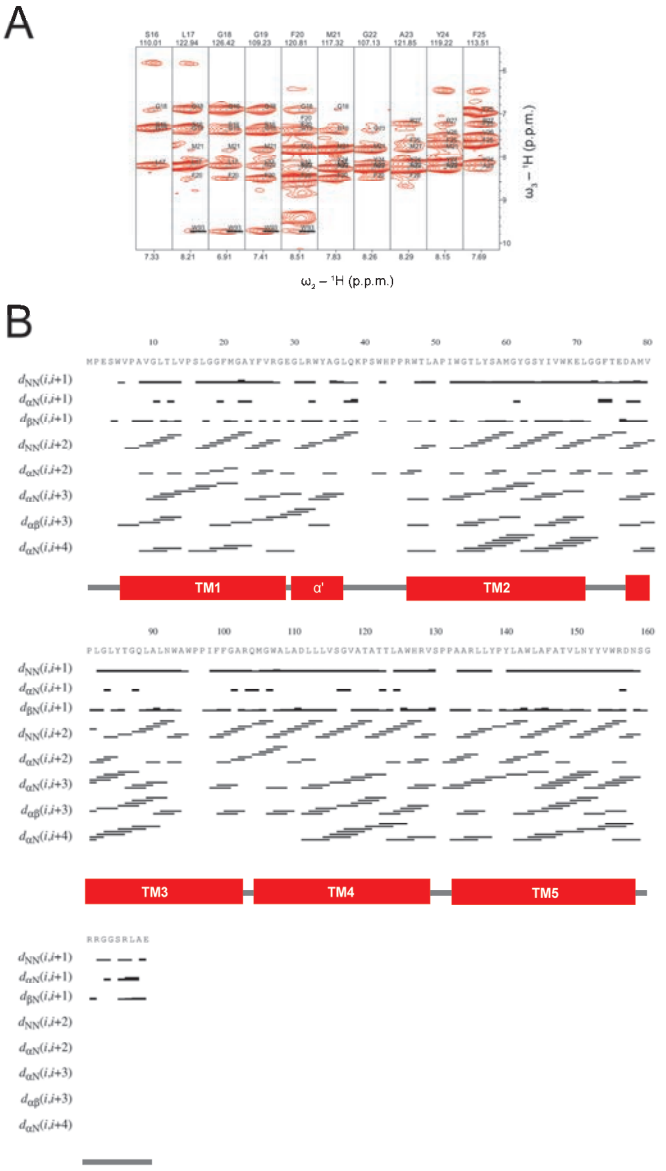

Fig. S3

Sequence-specific backbone assignment and NOE patterns. (A) Strips from a 3D ^{15}N-edited NOESY-HSQC (NOE mixing time of 200 ms; U-[^{2}H,^{15}N]-mTSPO-PK11195) highlighting the assignment of the TM1 region (S16-F25) of TSPO. In addition, long-range contacts between TM1 (L17-F20) and TM3 (side chain Hε1 of W93; underlined) are visible. **(B)** NOE contacts defining the secondary structure of mTSPO in complex with PK11195.

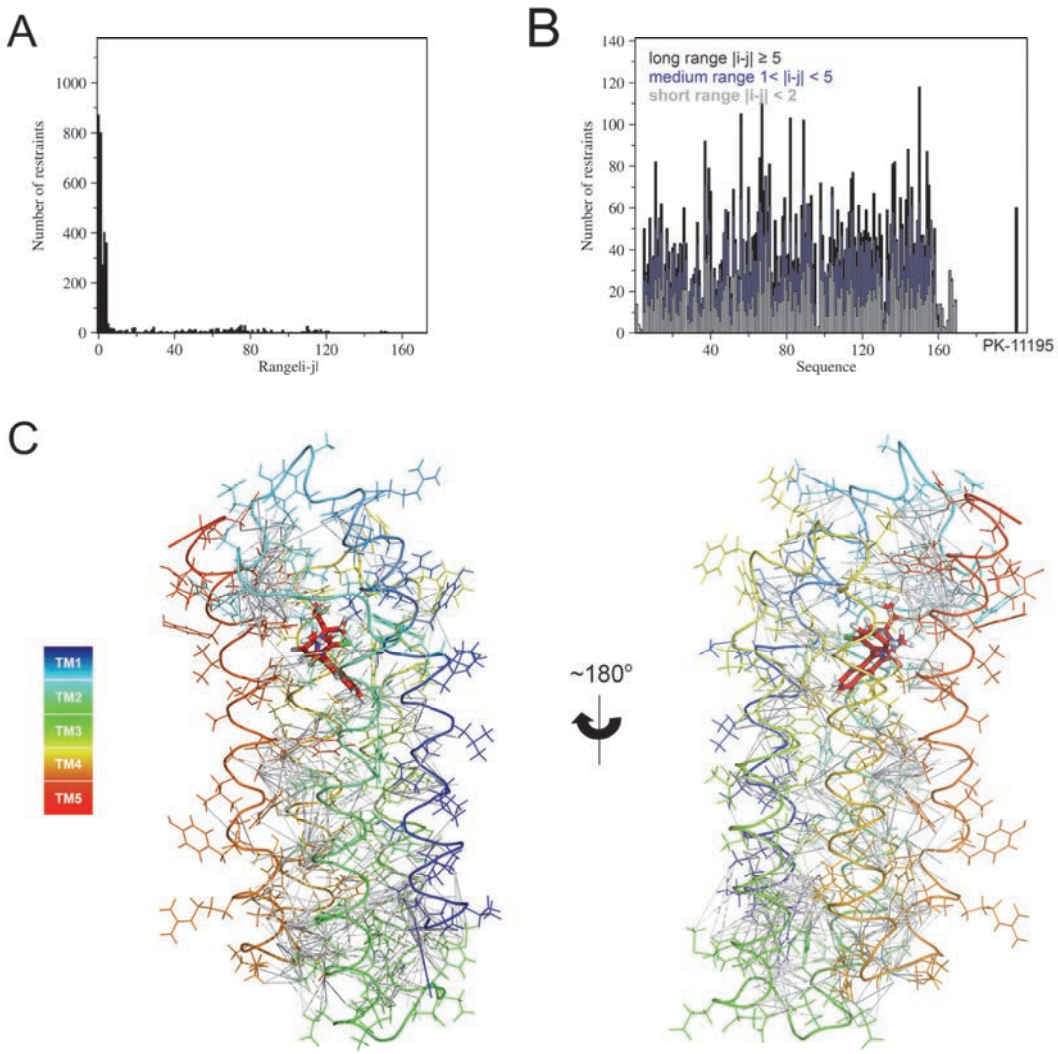

Fig. S4

Statistics of NOE restraints. **(A)** Number of NOE-derived restraints used in the structure determination of the mTSPO-PK11195 complex as a function of the sequence separation of the involved protons. **(B)** Number of short-, medium- and long-range NOE-derived restraints as a function of residue number. The number of TSPO-to-PK11195 contacts is shown as black bar. (**C**) Network of long-range intraprotein NOEs (grey lines) mapped onto the 3D structure of the mTSPO-PK11195 complex.

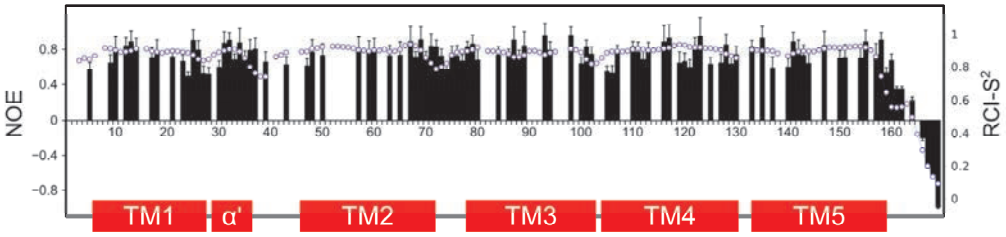

Fig. S5

Backbone dynamics of mTSPO in complex with PK11195. ^{1}H-^{15}N steady-state NOEs (black bars) were acquired with a recycle delay of d_1 = 10 s on a 700 MHz spectrometer. Error bars were calculated according to $\Delta NOE_i = |NOE_i| \cdot [1/(S/N_{NOEi})^2 + 1/(S/N_{noNOEi})^2]^{1/2}$, with $NOE_i = I_{NOEi}/I_{noNOEi}$, S/N the signal-to-noise ratio, and I_{NOEi} and I_{noNOEi} the peak heights with and without presaturation, respectively. Only NOE values of residues with well-separated cross peaks and with $\Delta NOE_i/|NOE_i|*100\% < 25\%$ are shown. Residue-specific RCI-S^2 order parameters, which were calculated from backbone chemical shifts, are shown as open circles.

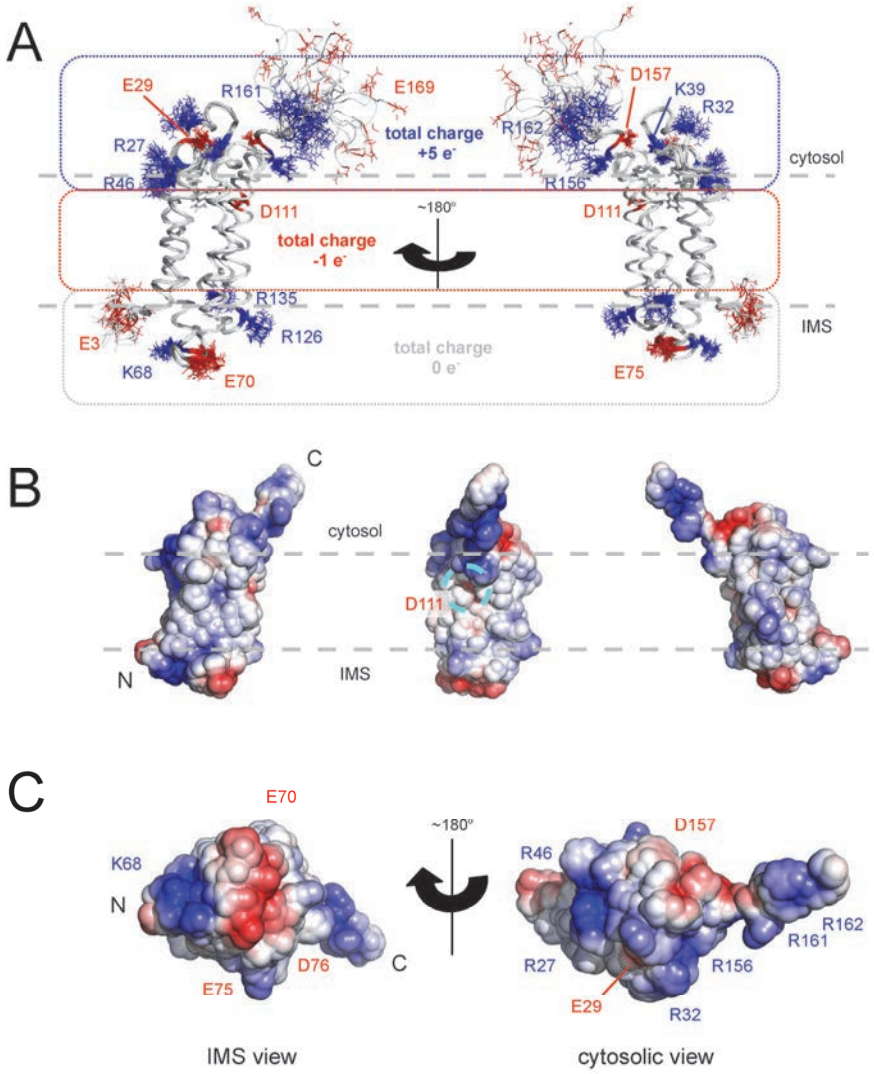

Fig. S6

Distribution of charged residues in the mTSPO-PK11195 structure. (A) Backbone trace with positively charged side chains shown in blue (R+K) and negatively charged ones in red (D+E). Dashed horizontal lines indicate the approximate membrane boundaries. Net charges are calculated within the dotted rectangles for the complex part pointing towards the cytosol (blue), inside the membrane (red), and towards the IMS (light gray). **(B)** Van der Waals surface of the mTSPO-PK11195 complex colored according to the electrostatic surface potential. The electrostatic surface potential was calculated using APBS(*45*). Positive and negative charges are shown in blue and red, respectively. The dotted cyan circle marks the location of the negative side chain of D111. **(C)** IMS and cytosolic views of the positive and negative patches in the mTSPO-PK11195 structure.

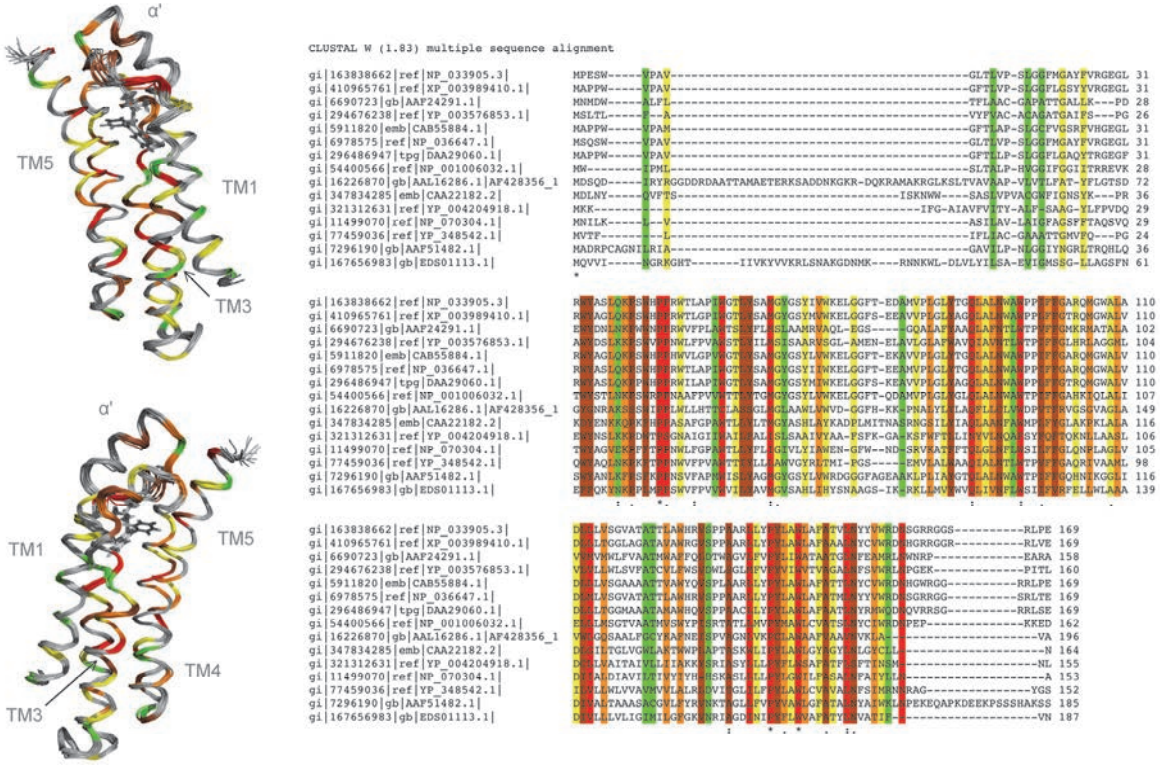

Fig. S7

Sequence conservation of TSPO. (left) Mapping of evolutionary conserved residues onto the 3D structure of the mTSPO-PK11195 complex. The level of sequence conservation decreases with a color gradient from red to green. (right) Sequence alignment of TSPO from different organisms: *Mus musculus* (NP_033905.3), *Felis catus* (XP_003989410.1), *Rhodobacter sphaeroides* (AAF24291.1), *Rhodobacter capsulatus* SB 1003 (YP_003576853.1), *Homo sapiens* (CAB55884.1), *Rattus norvegicus* (NP_036647.1), *Bos taurus* (DAA29060.1), *Danio rerio* (NP_001006032.1), *Arabidopsis thaliana* (AAL16286.1), *Schizosaccharomyces pombe* (CAA22182.2), *Bacillus subtilis* BSn5 (YP_004204918.1), *Archaeoglobus fulgidus* DSM 4304 (NP_070304.1), *Pseudethanolomonas fluorescens* Pf0-1 (YP_348542.1), *Drosophila melanogaster* (AAF51482.1), *Eubacterium siraeum* DSM 15702 (EDS01113.1).

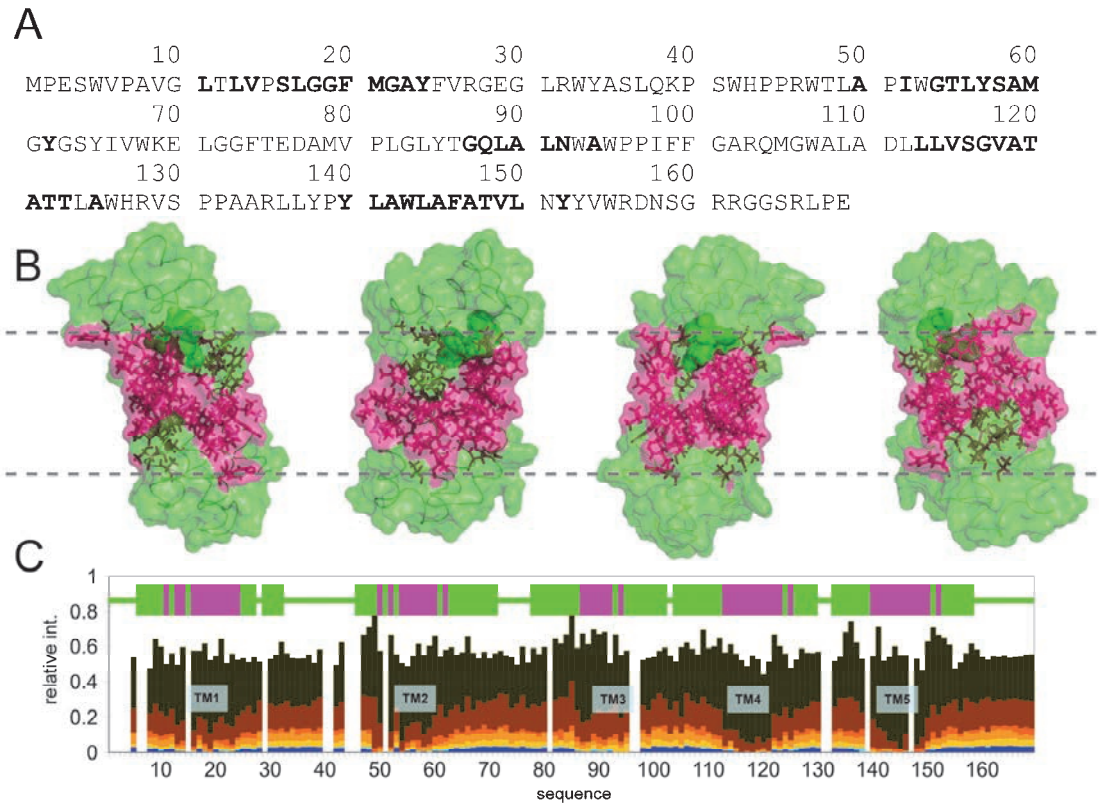

Fig. S8

Paramagnetic relaxation enhancement of mTSPO by spin-labeled detergent. (A) Primary sequence of mTSPO with residues having a relaxation enhancement of $\varepsilon > 20\ s^{-1}\ mM^{-1}$ shown in bold. Relaxation enhancement rates were determined from 2D ^{1}H-^{15}N HSQC spectra by titration of the mTSPO-PK11195 complex with increasing concentrations of *16*-Doxyl-stearic acid (2-(14-carboxytetradecyl)-2-ethyl-4,4-dimethyl-3-oxazolidinyloxy, free radical; Aldrich). **(B)** The same residues that are bold in (a) are mapped in magenta onto the mTSPO-PK11195 complex structure and their side chains are shown with sticks. Residues with $\varepsilon \leq 20\ s^{-1}\ mM^{-1}$ are shown using a green van der Waals surface. PK11195 atoms are represented by dark green spheres. Four different orientations rotated by 90° are shown. **(C)** Relative intensities of the N/NH correlation cross peaks observed in 2D ^{1}H-^{15}N HSQC spectra in the presence of 0.5 mM (brown), 2.5 mM (red), 3.5 mM (orange), 4.5 mM (light orange), 5.5 mM (yellow), 6.5 mM (cyan), and 8.5 mM (blue) *16*-Doxyl-stearic acid. The locations of the five TM helices are shown in green. Residues with $\varepsilon > 20\ s^{-1}\ mM^{-1}$ – that are located exclusively in the center of the TM helices – are represented in magenta.

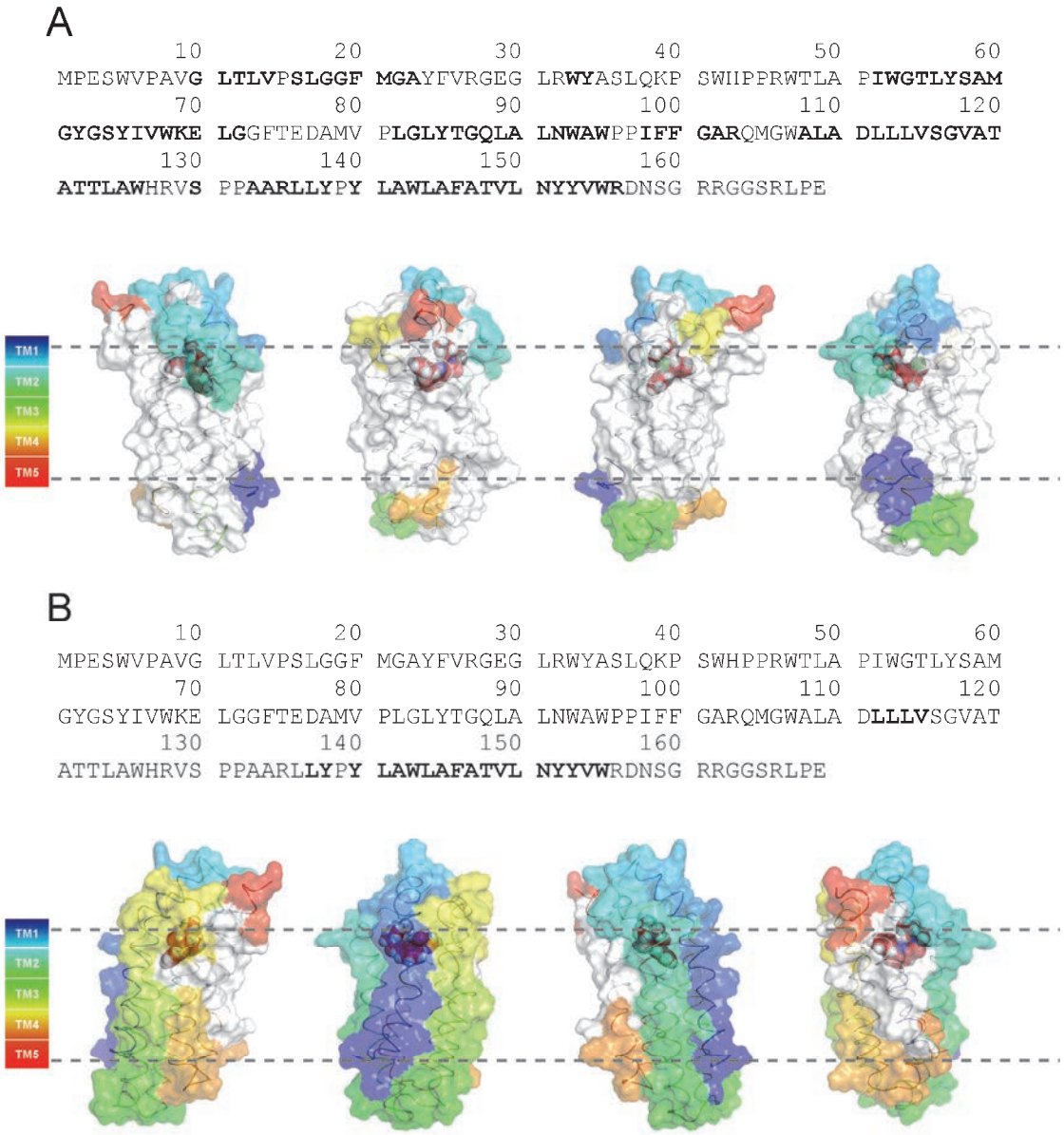

Fig. S9

Hydrogen/deuterium exchange of mTSPO-PK11195. The residues of the mTSPO-PK11195 complex, for which cross-peaks were observed in 2D ^{1}H-^{15}N HSQC spectra after 8 h **(A)** and 28 h **(B)** of exchange in D_2O, are bold in the primary sequence and mapped in white onto the 3D structure. The rest of the complex structure is colored according to the color scheme on the left. Four different orientations of the mTSPO-PK11195 structure are shown. Dotted lines indicate the approximate membrane boundaries.

Table S1.

NMR constraints and structural statistics for the ensemble of 20 lowest-energy structures of the mTSPO-PK11195 complex.

NMR distance & dihedral constraints	
NOE distance constraints[a)]	
Total NOE	3362
intraresidual (|*i-j*| = 0)	878
sequential (|*i-j*| = 1)	797
medium-range (1 < |i-j| < 5)	996
long-range (|i-j| ≥ 5)	630
protein to ligand	61
NOE restraints/residue	19.9
Hydrogen bonds restraints	170
Torsion angle constraints	
backbone (φ/ψ)	138/137
Structure Statistics	
Mean r.m.s.d. from exp. restraints (± s.d.)[b)]	
NOE (Å)	0.0017 ± 0.0002
dihedral angles (deg)	0.4341 ± 0.0548
Deviations from idealized geometry	
Bond lengths (Å) · 10^{-3}	2.531 ± 0.049
Bond angles (deg)	0.498 ± 0.004
Impropers (deg)	0.303 ± 0.007
r.m.s.d. to the first structure	
backbone atoms (5-28...47-159) (Å)	0.58 ± 0.10
heavy atoms (5-28...47-159) (Å)	1.15 ± 0.15
Ramachandran plot (5-28...47-159)	
most favored region	91.9%
additionally allowed region	7.8%
generously allowed region	0.3%

a) 20 lowest-energy structures out of 105 submitted to structure calculation.
b) None of the structures exhibited distance violations greater than 0.5 Å or dihedral angle violations > 5°.

References

1. V. Papadopoulos, M. Baraldi, T. R. Guilarte, T. B. Knudsen, J. J. Lacapère, P. Lindemann, M. D. Norenberg, D. Nutt, A. Weizman, M. R. Zhang, M. Gavish, Translocator protein (18 kDa): New nomenclature for the peripheral-type benzodiazepine receptor based on its structure and molecular function. *Trends Pharmacol. Sci.* **27**, 402–409 (2006). doi:10.1016/j.tips.2006.06.005 Medline

2. R. Rupprecht, V. Papadopoulos, G. Rammes, T. C. Baghai, J. Fan, N. Akula, G. Groyer, D. Adams, M. Schumacher, Translocator protein (18 kDa) (TSPO) as a therapeutic target for neurological and psychiatric disorders. *Nat. Rev. Drug Discov.* **9**, 971–988 (2010). doi:10.1038/nrd3295 Medline

3. J. Fan, P. Lindemann, M. G. Feuilloley, V. Papadopoulos, Structural and functional evolution of the translocator protein (18 kDa). *Curr. Mol. Med.* **12**, 369–386 (2012). Medline

4. C. Braestrup, R. F. Squires, Specific benzodiazepine receptors in rat brain characterized by high-affinity (^{3}H)diazepam binding. *Proc. Natl. Acad. Sci. U.S.A.* **74**, 3805–3809 (1977). doi:10.1073/pnas.74.9.3805 Medline

5. L. Veenman, V. Papadopoulos, M. Gavish, Channel-like functions of the 18-kDa translocator protein (TSPO): Regulation of apoptosis and steroidogenesis as part of the host-defense response. *Curr. Pharm. Des.* **13**, 2385–2405 (2007). doi:10.2174/138161207781368710 Medline

6. L. Veenman, M. Gavish, The role of 18 kDa mitochondrial translocator protein (TSPO) in programmed cell death, and effects of steroids on TSPO expression. *Curr. Mol. Med.* **12**, 398–412 (2012). Medline

7. W. Frank, K. M. Baar, E. Qudeimat, M. Woriedh, A. Alawady, D. Ratnadewi, L. Gremillon, B. Grimm, R. Reski, A mitochondrial protein homologous to the mammalian peripheral-type benzodiazepine receptor is essential for stress adaptation in plants. *Plant J.* **51**, 1004–1018 (2007). doi:10.1111/j.1365-313X.2007.03198.x Medline

8. A. M. Scarf, L. M. Ittner, M. Kassiou, The translocator protein (18 kDa): Central nervous system disease and drug design. *J. Med. Chem.* **52**, 581–592 (2009). doi:10.1021/jm8011678 Medline

9. R. Rupprecht, G. Rammes, D. Eser, T. C. Baghai, C. Schüle, C. Nothdurfter, T. Troxler, C. Gentsch, H. O. Kalkman, F. Chaperon, V. Uzunov, K. H. McAllister, V. Bertaina-Anglade, C. D. La Rochelle, D. Tuerck, A. Floesser, B. Kiese, M. Schumacher, R. Landgraf, F. Holsboer, K. Kucher, Translocator protein (18 kD) as target for anxiolytics without benzodiazepine-like side effects. *Science* **325**, 490–493 (2009). doi:10.1126/science.1175055 Medline

10. D. R. Owen, P. M. Matthews, Imaging brain microglial activation using positron emission tomography and translocator protein-specific radioligands. *Int. Rev. Neurobiol.* **101**, 19–39 (2011). doi:10.1016/B978-0-12-387718-5.00002-X Medline

11. J. J. Lacapère, F. Delavoie, H. Li, G. Péranzi, J. Maccario, V. Papadopoulos, B. Vidic, Structural and functional study of reconstituted peripheral benzodiazepine receptor. *Biochem. Biophys. Res. Commun.* **284**, 536–541 (2001). doi:10.1006/bbrc.2001.4975 Medline

12. K. E. Krueger, V. Papadopoulos, Peripheral-type benzodiazepine receptors mediate translocation of cholesterol from outer to inner mitochondrial membranes in adrenocortical cells. *J. Biol. Chem.* **265**, 15015–15022 (1990). Medline

13. V. Papadopoulos, A. G. Mukhin, E. Costa, K. E. Krueger, The peripheral-type benzodiazepine receptor is functionally linked to Leydig cell steroidogenesis. *J. Biol. Chem.* **265**, 3772–3779 (1990). Medline

14. A. M. Barron, L. M. Garcia-Segura, D. Caruso, A. Jayaraman, J. W. Lee, R. C. Melcangi, C. J. Pike, Ligand for translocator protein reverses pathology in a mouse model of Alzheimer's disease. *J. Neurosci.* **33**, 8891–8897 (2013). doi:10.1523/JNEUROSCI.1350-13.2013 Medline

15. J. Gatliff, M. Campanella, The 18 kDa translocator protein (TSPO): A new perspective in mitochondrial biology. *Curr. Mol. Med.* **12**, 356–368 (2012). Medline

16. E. Joseph-Liauzun, P. Delmas, D. Shire, P. Ferrara, Topological analysis of the peripheral benzodiazepine receptor in yeast mitochondrial membranes supports a five-transmembrane structure. *J. Biol. Chem.* **273**, 2146–2152 (1998). doi:10.1074/jbc.273.4.2146 Medline

17. S. Murail, J. C. Robert, Y. M. Coïc, J. M. Neumann, M. A. Ostuni, Z. X. Yao, V. Papadopoulos, N. Jamin, J. J. Lacapère, Secondary and tertiary structures of the transmembrane domains of the translocator protein TSPO determined by NMR. Stabilization of the TSPO tertiary fold upon ligand binding. *Biochim. Biophys. Acta* **1778**, 1375–1381 (2008). doi:10.1016/j.bbamem.2008.03.012 Medline

18. V. M. Korkhov, C. Sachse, J. M. Short, C. G. Tate, Three-dimensional structure of TspO by electron cryomicroscopy of helical crystals. *Structure* **18**, 677–687 (2010). doi:10.1016/j.str.2010.03.001 Medline

19. H. Li, V. Papadopoulos, Peripheral-type benzodiazepine receptor function in cholesterol transport. Identification of a putative cholesterol recognition/interaction amino acid sequence and consensus pattern. *Endocrinology* **139**, 4991–4997 (1998). Medline

20. F. Shah, S. P. Hume, V. W. Pike, S. Ashworth, J. McDermott, Synthesis of the enantiomers of [*N*-methyl-^{11}C]PK 11195 and comparison of their behaviours as radioligands for PK binding sites in rats. *Nucl. Med. Biol.* **21**, 573–581 (1994). doi:10.1016/0969-8051(94)90022-1 Medline

21. See supplementary materials on *Science* Online.

22. J. Liu, M. B. Rone, V. Papadopoulos, Protein-protein interactions mediate mitochondrial cholesterol transport and steroid biosynthesis. *J. Biol. Chem.* **281**, 38879–38893 (2006). doi:10.1074/jbc.M608820200 Medline

23. F. Delavoie, H. Li, M. Hardwick, J. C. Robert, C. Giatzakis, G. Péranzi, Z. X. Yao, J. Maccario, J. J. Lacapère, V. Papadopoulos, In vivo and in vitro peripheral-type benzodiazepine receptor polymerization: Functional significance in drug ligand and cholesterol binding. *Biochemistry* **42**, 4506–4519 (2003). doi:10.1021/bi0267487 Medline

24. Y. S. Lee, F. G. Siméon, E. Briard, V. W. Pike, Solution structures of the prototypical 18 kDa translocator protein ligand, PK 11195, elucidated with ^{1}H/^{13}C NMR spectroscopy and quantum chemistry. *ACS Chem. Neurosci.* **3**, 325–335 (2012). doi:10.1021/cn3000108 Medline

25. D. R. Owen, R. N. Gunn, E. A. Rabiner, I. Bennacef, M. Fujita, W. C. Kreisl, R. B. Innis, V. W. Pike, R. Reynolds, P. M. Matthews, C. A. Parker, Mixed-affinity binding in humans with 18-kDa translocator protein ligands. *J. Nucl. Med.* **52**, 24–32 (2011). doi:10.2967/jnumed.110.079459 Medline

26. R. Farges, E. Joseph-Liauzun, D. Shire, D. Caput, G. Le Fur, P. Ferrara, Site-directed mutagenesis of the peripheral benzodiazepine receptor: Identification of amino acids implicated in the binding site of Ro5-4864. *Mol. Pharmacol.* **46**, 1160–1167 (1994). Medline

27. N. Jamin, J. M. Neumann, M. A. Ostuni, T. K. Vu, Z. X. Yao, S. Murail, J. C. Robert, C. Giatzakis, V. Papadopoulos, J. J. Lacapère, Characterization of the cholesterol recognition amino acid consensus sequence of the peripheral-type benzodiazepine receptor. *Mol. Endocrinol.* **19**, 588–594 (2005). doi:10.1210/me.2004-0308 Medline

28. E. A. Morrison, K. A. Henzler-Wildman, Reconstitution of integral membrane proteins into isotropic bicelles with improved sample stability and expanded lipid composition profile. *Biochim. Biophys. Acta* **1818**, 814–820 (2012). doi:10.1016/j.bbamem.2011.12.020 Medline

29. R. Keller, thesis, ETH Zürich (2005); www.cara.nmr-software.org/downloads/NMR.017-1.1_Online.pdf.

30. M. Salzmann, K. Pervushin, G. Wider, H. Senn, K. Wüthrich, TROSY in triple-resonance experiments: New perspectives for sequential NMR assignment of large proteins. *Proc. Natl. Acad. Sci. U.S.A.* **95**, 13585–13590 (1998). doi:10.1073/pnas.95.23.13585 Medline

31. K. Pervushin, R. Riek, G. Wider, K. Wüthrich, Attenuated T2 relaxation by mutual cancellation of dipole-dipole coupling and chemical shift anisotropy indicates an avenue to NMR structures of very large biological macromolecules in solution. *Proc. Natl. Acad. Sci. U.S.A.* **94**, 12366–12371 (1997). doi:10.1073/pnas.94.23.12366 Medline

32. A. Bax, Multidimensional nuclear-magnetic-resonance methods for protein studies. *Curr. Opin. Struct. Biol.* **4**, 738–744 (1994). doi:10.1016/S0959-440X(94)90173-2

33. R. Riek, G. Wider, K. Pervushin, K. Wüthrich, Polarization transfer by cross-correlated relaxation in solution NMR with very large molecules. *Proc. Natl. Acad. Sci. U.S.A.* **96**, 4918–4923 (1999). doi:10.1073/pnas.96.9.4918 Medline

34. K. Wuthrich, *NMR of Proteins and Nucleic Acids* (Wiley Interscience, New York, 1986).

35. D. Marion, P. C. Driscoll, L. E. Kay, P. T. Wingfield, A. Bax, A. M. Gronenborn, G. M. Clore, Overcoming the overlap problem in the assignment of ^{1}H NMR spectra of larger proteins by use of three-dimensional heteronuclear ^{1}H-^{15}N Hartmann-Hahn-multiple quantum coherence and nuclear Overhauser-multiple quantum coherence spectroscopy: Application to interleukin 1β. *Biochemistry* **28**, 6150–6156 (1989). doi:10.1021/bi00441a004 Medline

36. Y. Shen, A. Bax, Prediction of Xaa-Pro peptide bond conformation from sequence and chemical shifts. *J. Biomol. NMR* **46**, 199–204 (2010). doi:10.1007/s10858-009-9395-y Medline

37. A. Bax, G. M. Clore, A. M. Gronenborn, ^{1}H-^{1}H correlation via isotropic mixing of ^{13}C magnetization, a new 3-dimensional approach for assigning ^{1}H and ^{13}C spectra of ^{13}C-enriched proteins. *J. Magn. Reson.* **88**, 425 (1990). doi:10.1016/0022-2364(90)90202-K

38. P. Lundström, K. Teilum, T. Carstensen, I. Bezsonova, S. Wiesner, D. F. Hansen, T. L. Religa, M. Akke, L. E. Kay, Fractional ^{13}C enrichment of isolated carbons using [1-^{13}C]- or [2-^{13}C]-glucose facilitates the accurate measurement of dynamics at backbone Cα and side-chain methyl positions in proteins. *J. Biomol. NMR* **38**, 199–212 (2007). doi:10.1007/s10858-007-9158-6 Medline

39. C. Zwahlen, P. Legault, S. J. F. Vincent, J. Greenblatt, R. Konrat, L. E. Kay, Methods for measurement of intermolecular NOEs by multinuclear NMR spectroscopy: Application to a bacteriophage lambda N-peptide/boxB RNA complex. *J. Am. Chem. Soc.* **119**, 6711–6721 (1997). doi:10.1021/ja970224q

40. P. Güntert, Automated NMR structure calculation with CYANA. *Methods Mol. Biol.* **278**, 353–378 (2004). Medline

41. Y. Shen, F. Delaglio, G. Cornilescu, A. Bax, TALOS+: A hybrid method for predicting protein backbone torsion angles from NMR chemical shifts. *J. Biomol. NMR* **44**, 213–223 (2009). doi:10.1007/s10858-009-9333-z Medline

42. C. D. Schwieters, J. J. Kuszewski, N. Tjandra, G. M. Clore, The Xplor-NIH NMR molecular structure determination package. *J. Magn. Reson.* **160**, 65–73 (2003). doi:10.1016/S1090-7807(02)00014-9 Medline

43. N. A. Farrow, R. Muhandiram, A. U. Singer, S. M. Pascal, C. M. Kay, G. Gish, S. E. Shoelson, T. Pawson, J. D. Forman-Kay, L. E. Kay, Backbone dynamics of a free and phosphopeptide-complexed Src homology 2 domain studied by ^{15}N NMR relaxation. *Biochemistry* **33**, 5984–6003 (1994). doi:10.1021/bi00185a040 Medline

44. M. V. Berjanskii, D. S. Wishart, A simple method to predict protein flexibility using secondary chemical shifts. *J. Am. Chem. Soc.* **127**, 14970–14971 (2005). doi:10.1021/ja054842f Medline

45. N. A. Baker, D. Sept, S. Joseph, M. J. Holst, J. A. McCammon, Electrostatics of nanosystems: Application to microtubules and the ribosome. *Proc. Natl. Acad. Sci. U.S.A.* **98**, 10037–10041 (2001). doi:10.1073/pnas.181342398 Medline